metals

MDPI

Article

Low Frequency Giant Magneto-Impedance Effect of Co-Rich Ribbons Induced by Joule Annealing Treatment

Shuling Zhang [1,*], Zhiying Gan [1], Weiye Chen [2] and Dawei Zhao [3]

[1] School of Mechanical and Automotive Engineering, Qingdao University of Technology, Qingdao 266520, China
[2] School of Materials Science and Engineering, North Minzu University, Yinchuan 750021, China
[3] Department of Welding Engineering, Institution of Engineering and Technology, South Ural State University, Chelyabinsk 454080, Russia
* Correspondence: zhangshuling@qut.edu.cn; Tel.: +86-17861420579

Abstract: The giant magneto-impedance (GMI) effect of $Co_{83.2}Fe_{5.2}Si_{8.8}B_{2.8}$ ribbons at frequencies of <1 MHz was analyzed. To improve the GMI response, a Joule annealing treatment was conducted with a direct current, and the domain structure of the ribbon surface was investigated via magneto-optical Kerr effect microscopy. The annealed ribbons show larger impedance changes under external magnetic fields, and higher field sensitivity is obtained by certain current annealing treatments. The field sensitivity of 418 and 782%/(kA/m) at 0.2 MHz and 0.8 MHz are achieved after annealing at 0.8 A for 20 min. The annealing treatment under direct electric current induces stress relaxation, and domain rearrangement, and the crystallization process gradually increases with the increasing current density, which gives rise to anisotropic reformation. The release of stresses due to Joule heating below the crystallization temperature causes the homogenous distribution of stress induced by rapid solidification and influences the elastic anisotropy, causing the domain structures to become much more regular. The crystallization, along with the precipitation of hard magnetic phases, increases the crystal anisotropy and induces the intense magnetic coupling action. Consequently, the magnetic domains in the annealed ribbons are rearranged with reformed anisotropy by Joule annealing heat and by the transverse magnetic field induced by the current. The irregular domains, with complex anisotropy in the as-cast ribbons corresponding to the weak GMI response, are transformed into regular and strip-like domains, with transverse easy magnetization after annealing at 0.4 A. After annealing at 0.8 A, the domains are further transformed into fine axial fingerprint-like domains, which are much more sensitive to the change in the axial external magnetic field, allowing for the best GMI response. These results indicate that the Joule annealing treatment is an optional method to optimize the soft magnetic properties and the GMI effect of these Co-rich ribbons at low frequencies.

Keywords: GMI effect; domain structure; magnetization process; field sensitivity; Co-rich ribbon

check for updates

Citation: Zhang, S.; Gan, Z.; Chen, W.; Zhao, D. Low Frequency Giant Magneto-Impedance Effect of Co-Rich Ribbons Induced by Joule Annealing Treatment. *Metals* **2023**, *13*, 28. https://doi.org/10.3390/met13010028

Academic Editor: Aphrodite Ktena

Received: 1 November 2022
Revised: 16 December 2022
Accepted: 19 December 2022
Published: 22 December 2022

Copyright: © 2022 by the authors. Licensee MDPI, Basel, Switzerland. This article is an open access article distributed under the terms and conditions of the Creative Commons Attribution (CC BY) license (https://creativecommons.org/licenses/by/4.0/).

1. Introduction

In 1992, Mohri et al. found that CoFeSiB amorphous microwires exhibited impedance sensitivity to an external magnetic field and called this phenomenon the giant magneto-impedance (GMI) effect [1]. The sensitive response of the GMI effect, allowing for the sensor design to meter weak magnetic fields or stress, has received global attention [2–5]. The GMI effect has been observed in different kinds of materials, including ribbons, microwires, films, and sandwiches [6]. Among these, metallic magnetic ribbons have received more attention, owing to the mature preparation process, commercial mass production, and their wide technical applications. The magnetic softness and GMI effect of as cast ribbons are associated with both their amorphous state, which prevents the typical defects related to crystalline materials, and the distribution of residual strain originating from the rapid solidification process [7–9]. Moreover, the presence of spatially distributed tension in the ribbon-shaped

soft magnetic amorphous materials induces large transverse and longitudinal anisotropy fields related to the main GMI features. In addition, the magnetoelastic stress in the Co-rich ribbons determines their domain structures [10]. It is observed that domains distributed on the smooth ribbon surfaces contacted with the roller represent axial magnetization, with longitudinal anisotropy. However, domains on a ribbon surface separated from a roller represent transverse magnetization responsible for transverse magnetic anisotropy [10]. The dynamic process of magnetization is determined by the domain structures and their formation process [11,12]. The origin and the main characteristics of the GMI effect are theoretically explained in terms of classical electrodynamics, considering the magnetization process and the skin effect under a driving alternating current [7,13]. According to the skin effect theory, soft magnetic performance, especially high magnetic permeability, is important for the GMI effect [8,14]. Consequently, the observation of domain structures can reflect the magnetic softness to explore and analyze the GMI effect. It is also reported that there are fluctuations in the domain wall during the magnetization process, which significantly contributes to the intrinsic noise of the GMI sensors [2,15].

It is notable that a large and sensitive GMI effect is related to well established magnetic anisotropy. Therefore, to improve the soft magnetic performance and field sensitivity of the GMI response, diverse post-processes (heat treatments) are employed to improve the GMI effect by reducing the spatial distribution of stress and restraining the domains [16–18]. The magnetoelastic anisotropy determined by the internal stress distribution is affected by the chemical composition related to the magnetostriction coefficient and the solidification process. Therefore, Fe-rich and Co-rich amorphous alloys with a vanishing magnetostriction coefficient are most commonly reported for the optimization of magnetic softness and the GMI effect. However, most Fe-rich amorphous alloys and crystallized materials are rather brittle, and their technical applications are limited [19].

In particular, Joule current annealing is a convenient and operable technique to influence the magnetic performance of magnetic materials [5,20,21]. Up until now, the highest GMI effect, with $\triangle Z/Z$ up to 650%, has been experimentally reported in Co-rich glass-coated microwires after optimal Joule annealing treatment. The reason for these high $\triangle Z/Z$ values in these Co-rich microwires is due to better magnetic softness intrinsically related to the high internal stresses with thinner diameters, with the chemical composition of metallic alloy allowing for the achievement of the vanishing magnetostriction coefficient and the appropriate post processing conditions and sample geometry [22].

Stress and conventional annealing treatments were also carried out. It was found that the highest sensitivity of 104%/Oe and the highest GMI response of 234% at 100 MHz were achieved by stress-annealing in Co-rich glass-coated microwires [23]. The transverse Oersted magnetic field generated by the Joule current is considered to denote the potential change in domain structures and anisotropy under sufficiently high Joule heat [11,16]. The domain structures may be re-oriented and homogenized by the Joule annealing treatment under thermal energy and magnetic field induced by the electric currents [16]. In Co-rich microwires, a large and sensitive GMI at GHz frequencies is observed due to the formation of a circular magnetic field during the Joule heating [18]. For the Co-rich microwire annealed with a current of 90 mA, $\triangle Z/Z$ is increased by about 300% when a stress of 450 MPa is applied [24]. The GMI effect in ribbon-shaped materials is associated with the sensitivity of the transverse component of the magnetic susceptibility to the external magnetic field, and the Joule current annealing treatment improves the transverse magnetic anisotropy that enhances the mentioned circular susceptibility and the GMI response [20,25].

Consequently, studies on domain structures in Joule annealed Co-rich amorphous ribbons are relevant both for technological application and from the view of understanding the transformation of induced anisotropy to improve GMI response. Therefore, in this paper, Co-rich amorphous ribbons are annealed under different current amplitudes (0–1.0 A), and the dynamic evolution of the surface domain is investigated systematically via the magneto-

optical Kerr effect (MOKE) microscopy to analyze the structure transformation and establish its influence on the GMI effect.

2. Experimental Method and Details

Ribbons with a chemical composition $Co_{83.2}Fe_{5.2}Si_{8.8}B_{2.8}$ are fabricated by the melt-spinning technique using a single Cu wheel in a high purity Ar gas (99.99%) atmosphere. The ribbon is 28 μm thick and 0.8 mm in wide. Then ribbons are cut into 15 cm lengths for the Joule annealing treatments. The anneal currents are 0.2 A,0.4 A,0.6 A,0.8 A, and 1.0 A which corresponds to the current density of 8.9 A/mm^2, 17.9 A/mm^2, 26.8 A/mm^2, 35.7 A/mm^2, and 44.6 A/mm^2. The current density of Joule heating is selected according to the previously reported study on the Joule heating of amorphous materials [26]. Dealing with Joule annealing treatment, it is commonly accepted that the current density of 30–45 A/mm^2 produces heating up to 400 °C [18]. In ribbon-shaped magnetic materials, such values can be lower for the bulk volume and slower cooling rates. The ribbon surfaces of the non-contacted roller are attached to a disk with the length of 20 mm for domain observation utilizing a MOKE magnetic domain observation system (Evico, Germany). As previously mentioned, the GMI effect is driven by the transverse magnetic field induced by the current and the external magnetic field, H_{ex}, and the impedance measured changes with H_{ex}. To analyze the magnetization process, an axial H_{ex} is also used during the observation of the domain structure.

The GMI effect of Co-rich ribbons is measured using an impedance analyzer (Agilent 4294 A, America). The measured ribbon is 2 cm in length and is connected to the electric circuit by manual wielding. The driving frequency is 100 Hz to 110 MHz, and the current amplitude is kept at a constant value of 10 mA, far below the crystalline onset point. The applied H_{ex}, which is generated by a pair of Helmholtz coils, is swept from −7.2 KA/m to +7.2 KA/m. The GMI ratio is defined as:

$$\Delta Z/Z(\%) = [Z(H_{ex}) - Z(H_{max})] \times 100\%/Z(H_{max})] \quad (1)$$

where $Z(H_{ex})$ and $Z(H_{\max})$ are the impedance values at a specific H_{ex} and the maximum H_{ex} of 7.2 KA/m, separately.

In order to further describe the GMI response with the magnetic field, using the slope of GMI curve, the sensitivity S is defined as:

$$S = \frac{d(\Delta Z/Z)}{dH_{ex}} \quad (2)$$

During the impedance test, H_{ex} is paralleled to the longitudinal direction of the ribbon, which is perpendicular to the local surface magnetic field of the Earth to eliminate the external field influence.

An X-ray diffractometer (XRD) is used for phase identification (XRD-6000, Japan). The X-ray source is the Cu target and the Ka ray, with the characteristic wavelength of 0.1542 nm and the acceleration voltage of 40 KV, and the continuous scanning angle range is 10~80°, with a scanning angular velocity of 1°/min. A scanning electron microscope, SEM (SIGMA 500, Germany), is used to observe the ribbon surface morphology. The distribution of elements is also analyzed using an energy dispersive spectrometer (EDS) fitted with the SEM.

All the experimental tests are carried out at room temperature.

3. Results and Discussion

3.1. The Microstructure and GMI Effect

The XRD patterns of the ribbons, before and after current annealing, are shown in Figure 1. Although the diffraction intensity is weak due to the small area of the thin ribbon, it does not affect the comparation between different annealed samples for phase analysis. The XRD patterns of the as-cast ribbons exhibit only one broad halo peak at

around $2\theta = 45^\circ$, indicating the amorphous state of the casting sample. When the annealing current density is 0.4 A, there are weak and broadened diffraction peaks exhibiting the appearance of nano-micro particles in the annealed samples. As the annealing current is increased up to 1.0 A, there are many more crystalline diffraction peaks appearing from 40° to 80°, indicating the mass crystallization. Through Jade software analysis, the crystal phases obtained are mainly borides of cobalt and oxides of iron.

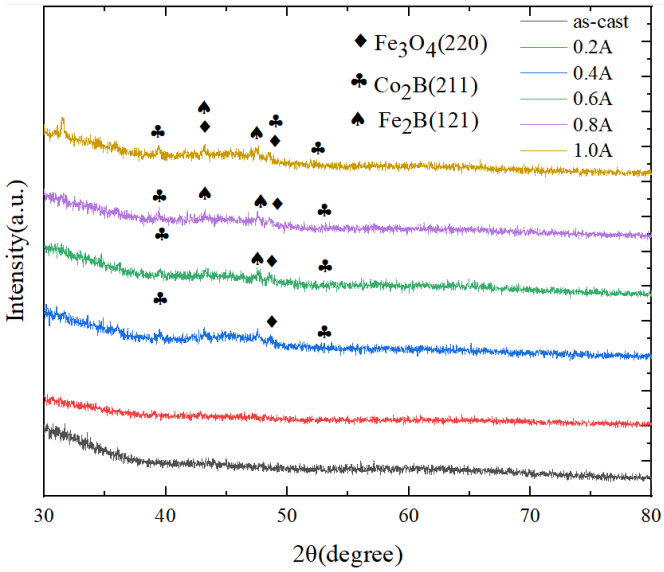


Figure 1. XRD patterns of as-cast and annealed ribbons.

The GMI response at different frequencies after Joule annealing is presented in Figure 2. The maximum GMI ratio is 3.2% at zero H_{ex} at 0.06 MHz, showing a single-peak feature, and the GMI effect in the as-cast ribbons is relatively weak. It can be seen, as frequency increases, two-peak GMI curves first appear in these annealed Co-rich ribbons. Even at 0.06 and 0.08 MHz, the GMI curves show two-peak features, and the maximum GMI ratios of 16.2% and 19.4% at 47.8 A/m and 63.7 A/m are also observed after annealing at 0.8 A for 20 min, as shown in Figure 2a,b. These phenomena can be interpreted by the skin effect and the change in transverse permeability influenced by the continuous change in H_{ex} [27]. At lower frequencies, the transverse permeability dominated by the magnetization under the ac current-induced transverse field reaches its peak when H_{ex} is near zero, which has little influence on the oscillating domain wall movement [25]. Consequently, the GMI effect is bell-shaped, showing a single peak feature. As the driving frequency increases along the ribbon, the skin effect becomes stronger, a decrease in the surface layer thickness is produced, and the permeability may drastically change. However, as the frequency increasing the magnetization process is blocked by the eddy current, a higher H_{ex} is required to rotate the magnetic moments, forming a transverse easy direction. The axial anisotropy can be compensated by the longitudinal H_{ex} when it reaches the switching field, at which time, the quasi-free magnetization responds quickly to the change in H_{ex} and induces the larger transverse permeability, as well as two GMI peaks at the positive and negative applied fields, respectively. The change in H_{ex} modifies the transverse permeability by the reorientation of the static magnetization and by the intrinsic field change of the permeability, simultaneously [26].

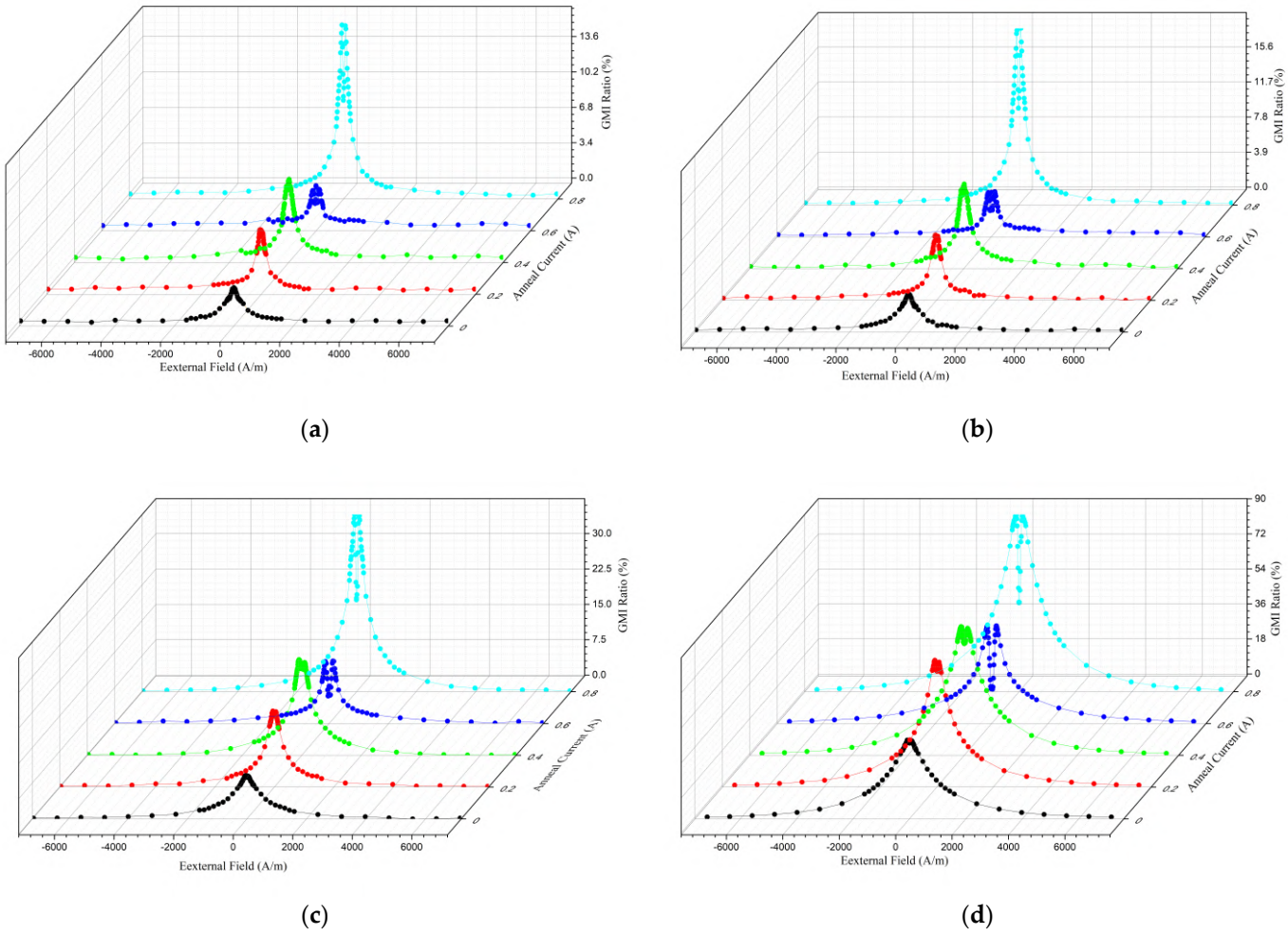


Figure 2. GMI curves of Co-rich as-cast and annealed ribbons at different frequencies: (**a**) 0.06 MHz, (**b**) 0.08 MHz, (**c**) 0.2 MHz, (**d**) 0.8 MHz.

It is known that the value of H_{ex}, where the electrical impedance presents a maximum value, is commonly linked to the average value of the anisotropy field or the effective anisotropy field, H_k, which is correlated to the peak position regarding the anisotropy distribution in the sample [10,28]. H_k, as a function of the annealing current density, is shown in Figure 3. At an annealing current of 0.6 A, H_k has the largest value at the same driving frequency, and the increase in H_k indicates an increase in the transverse anisotropy after Joule annealing treatments, which may correlate with the Joule heat and transvers magnetic field, both induced by the current. When the Joule heat is low and cannot induce crystallization, the inhomogeneous stress will be partially released, and the transverse anisotropy will be enhanced under the transvers magnetic field deduced by the Joule current. As the Joule current increases, the Joule heat is high enough to cause crystallization, and the magnetic anisotropy will change [5]. Moreover, to form the metallic compounds, the magnetic metallic elements of cobalt and iron should diffuse, which causes the inhomogeneous distribution of magnetic elements and gives rise to magnetic coupling. Consequently, the total anisotropy will be reformed.

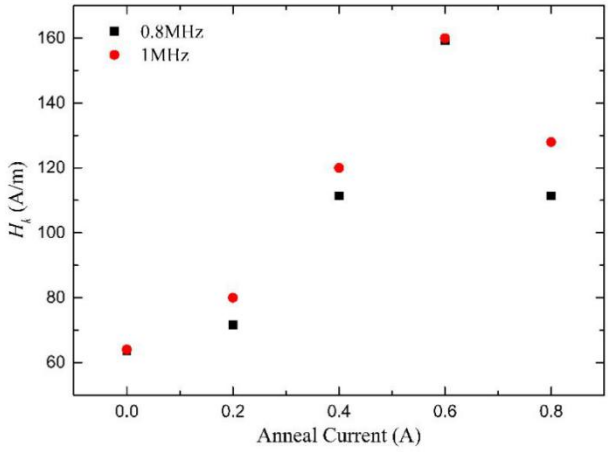


Figure 3. The effective anisotropy field, H_k.

The GMI effect on the annealed ribbons at different frequencies is summarized in Figure 4. There is an optimized frequency at which the GMI response is optimal, under our measured condition. At 0.2 MHz, the field sensitivities of the as-cast ribbons after annealing at 0.8 A are 16 and 418%/(kA/m), respectively. At 0.8 MHz, the field sensitivity increases from 46 to 782%/(kA/m).

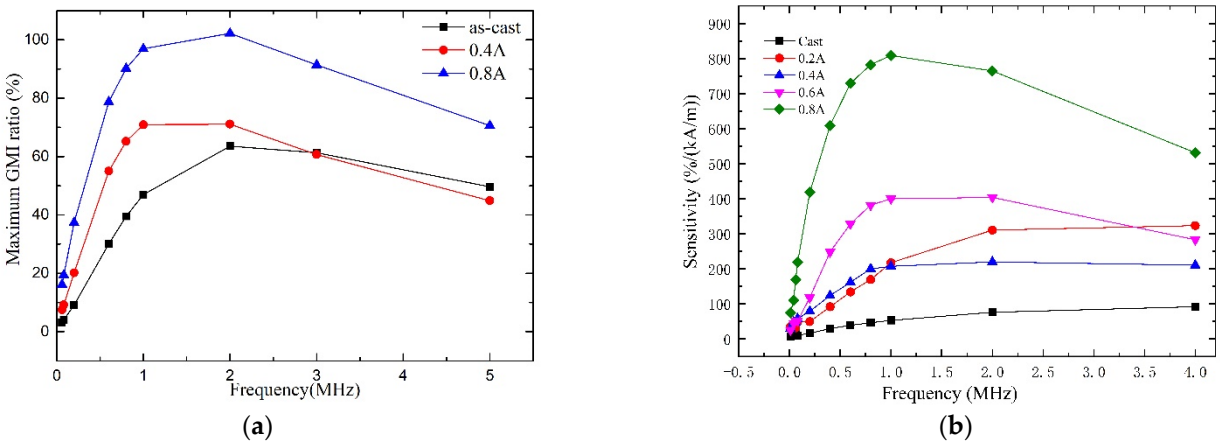


Figure 4. The maximum GMI (**a**) and field sensitivity (**b**) at different frequencies.

It has been previously reported that the sensitivity of 750%/(kA/m) at 0.8 MHz is obtained in nanocrystalline $Fe_{73.5}Cu_1Nb_3Si_{13.5}B_9$ ribbons annealed for 3–5 h at 550 °C with a maximum GMI ratio of 400% [7]. It can be noted that the reported sensitivity ranges from 240 A/m to 560 A/m, due to the nanocrystalline structure with larger anisotropy. Therefore, although the maximum GMI ratio at 0.8 MHz is 90% lower than the reported data, its sensitivity ranges from 16 to 48 A/m in a near zero magnetic field, and the field sensitivity is still higher. The highest GMI ratio of up to 650% is reported at 200 MHz in current annealed Co-rich microwires, and for as-cast wires, the highest GMI ratio of 550% is also observed at about 300 MHz [22]. Moreover, the largest magnetic field sensitivities of up to 10%/A/m are also reported in the Co-rich microwires [29]. Hence, these types of Co-rich microwires exhibit excellent GMI response, even in the as-cast state, and Joule current annealing is an effective method for treating these thin Co-rich ribbons in our experiments, which can effectively improve their low frequency GMI response. It should be mentioned that metallic amorphous microwires possess a single helical anisotropy, while amorphous ribbons show longitudinal and transverse anisotropy, due to the differences in morphology and domain structures [3]. Perhaps the difference in morphology and domain structures

is one of factors that determine the differences in the GMI effect between the microwires and ribbons.

The field sensitivity reaches the peak near 1 MHz and then decreases with a further increase in frequency. For the application of the GMI effect in sensors, the driving frequencies are expected to be low, without decreasing the GMI ratio, to avoid high-frequency magnetic intrinsic noise in the control systems. Consequently, the system noise and sensitivity can be more easily managed and controlled at low driving frequencies for GMI sensor [4].

3.2. Domain Structure Transformation

The GMI effect of Co-rich ribbons depends on the demagnetization process under the longitudinal magnetic field, and the transverse demagnetization field is particularly important [25,27]. The MOKE investigation on domain structures of the Co-rich amorphous ribbons provided relevant information regarding the surface domain structures and the magnetization reversal.

The domain structures of the as-cast ribbons are shown in Figure 5. The transformation of the domain structure under the H_{ex} is presented. The nucleation of the domain walls starts from the edges of ribbon, as shown in Figure 5a, and labeled as points A and B. When H_{ex} increases, nucleation is observed in the center, labeled C, D, and E in Figure 5b. The magnetic domain structure tends to saturate under the continuous increase in H_{ex}, which is related to the nonhomogeneous distribution of nucleation points in the ribbon surface. Notably, there are no regular banded domains observed, as previously reported, but rather crescent moon-shaped domains gradually appear on the surface of ribbons, as shown in Figure 5c. As H_{ex} increases, the magnetization is saturated, with many more domains forming, and pitting spots are observed on the original smooth surface, as shown in Figure 5d. It is determined that the cooling rate is much higher on the surface connected to the copper roller compared with the inner areas, which are the last areas to solidify. This may induce the different elastic anisotropies for the non-homogeneous stress distribution in the ribbon [10,11]. Additionally, the large temperature gradient during the formation of the amorphous ribbons also causes significant thermo-elastic strain and oscillation distribution of the stresses, which results in excess density of the defects and the heterogeneous domain structures [8]. To reduce the total system energy to achieve a thermodynamic stability, the transverse and axial anisotropy will coexist, inducing different domain structures in these ribbon surfaces. The diversity of the domain structures, lacking regulation, would lead to intense magnetic coupling interactions between the differently oriented structures during the magnetization process. When H_{ex} is high enough, the magnetization under axial H_{ex} would be saturated. The inner domains with axial orientation are observed as pitting points distributed on the ribbon surfaces. Therefore, diverse and irregular domain structures are observed in the as-cast ribbons. Consequently, there are many more blocks during the magnetization process, which also indicates the weak GMI response related to the fluctuations of the domain walls during the magnetization process.

The domain structures after Joule annealing treatment under H_{ex} are shown in Figure 6. Regular stripe-like domains are observed, with the gradually growth of a transverse easy magnetization direction, while the vortex domains shrink or diminish. Stripe-like domains of 180 μm width are slanted to the longitudinal direction after Joule annealing treatment at 0.2 A, and the angle between the strip and the axial of ribbon is ~60°. During long-time annealing, Joule heating will release a part of the casting stress, and the circular magnetic field generated by the annealing current can effectively improve the transverse anisotropy by constraining the orientation of the magnetic domain structures [16].

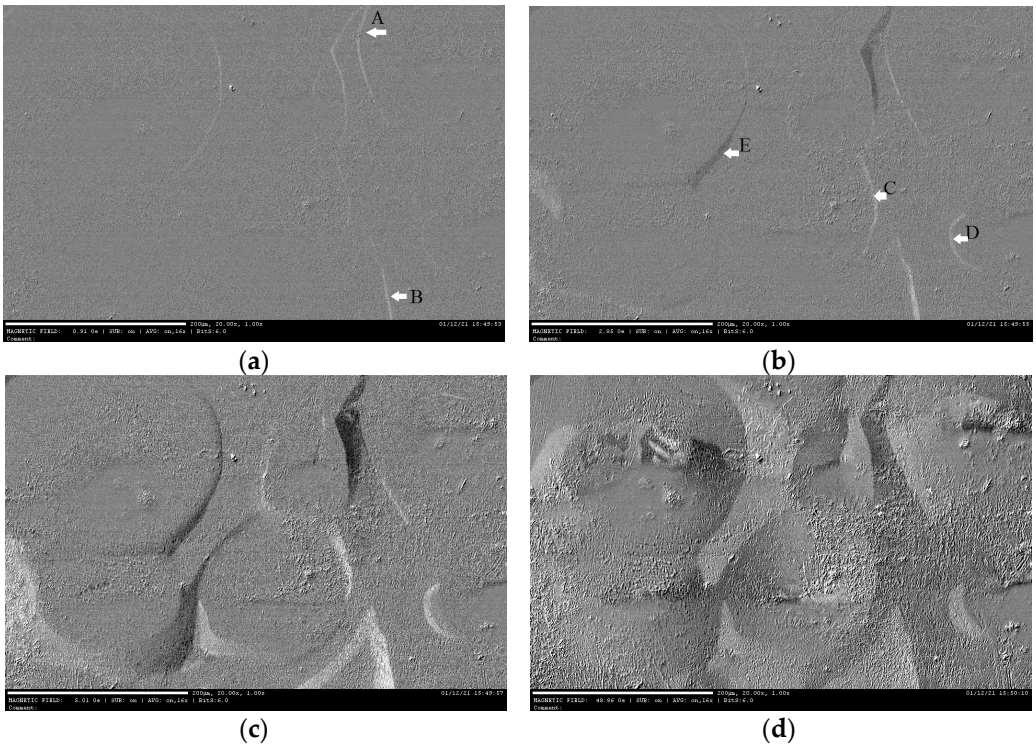


Figure 5. Surface domains of the as-cast ribbon under the axial applied magnetic field: (**a**) 72.8 A/m, (**b**) 228 A/m, (**c**) 425 A/m, (**d**) 3.9 KA/m. A and E present the nucleation of the domain walls starting from the edges of ribbon. C, D and E are fields that nucleation form in the center.

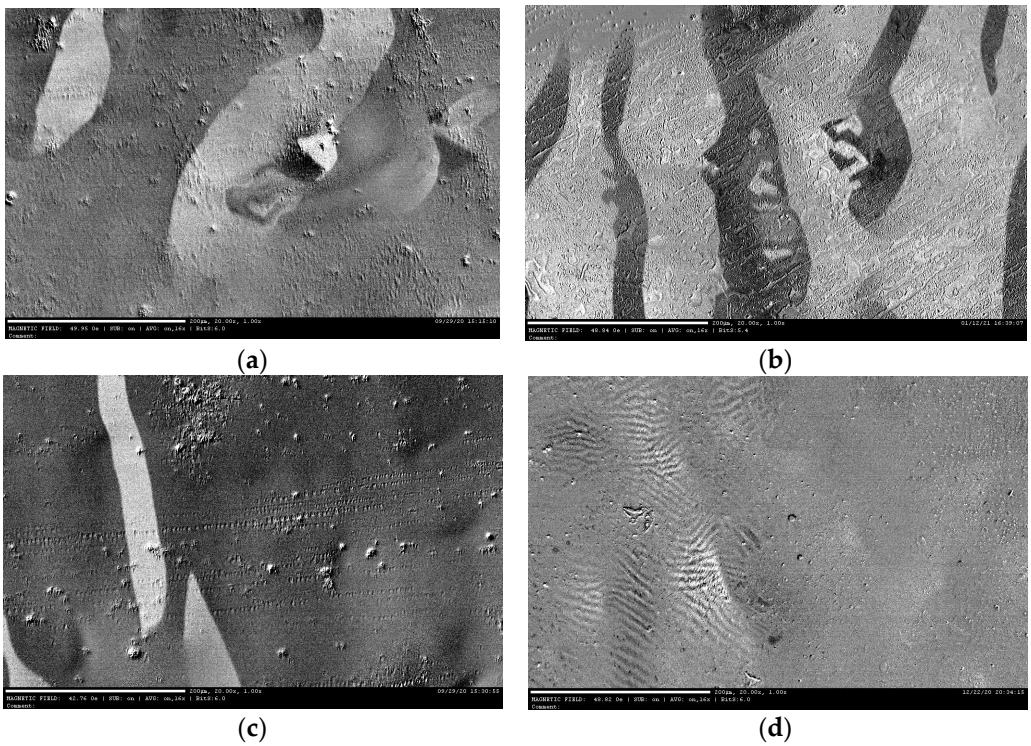


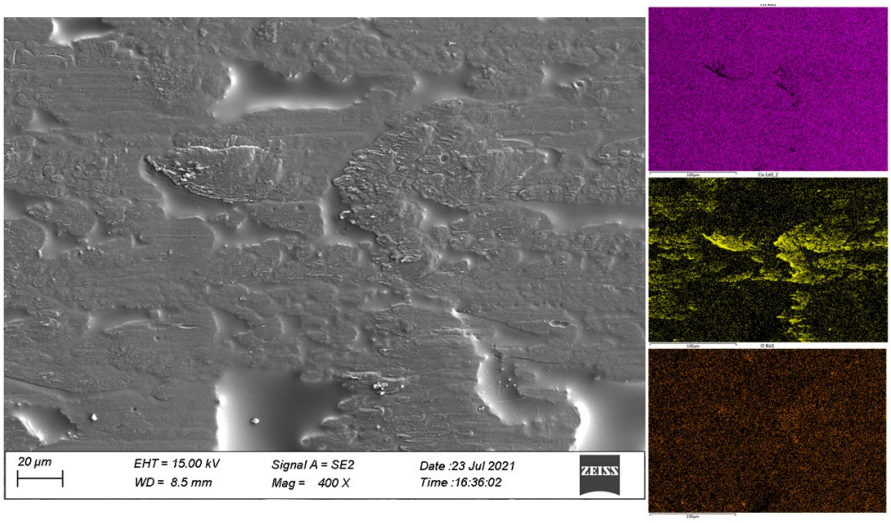
Figure 6. Surface domain structures under axial external magnetic field after annealing at different currents: (**a**) 0.2 A, (**b**) 0.4 A, (**c**) 0.6 A, (**d**) 0.8 A.

More regular strip-like transverse domain structures are presented after annealing at 0.4 A for 20 min, as shown in Figure 6b. The domain width is decreased to ~50 μm, and much clearer domain walls are observed between the domains with different orientations.

However, after annealing at 0.6 A, many thin stripe-like domains, with some bumps and pits, occur, and at an annealing current of 0.8 A, axial fine fingerprint-like domains are observed at the edges of the ribbons. These laminal domains are of ~8 μm thickness, occupying less than 50% of the observed surface, but no regular domains are observed in the left section; only bumps and pits. These domain structures may be related to the large local magnetic anisotropy due to local crystallization and surface oxide precipitation, as observed in Fe-rich nanocrystalline ribbons [7]. The incline of the domain structures to the ribbon axis indicates an increase in a transverse demagnetizing field. The existence of laminal domains means that a slight change in H_{ex} will trigger the rapid motion of the domain walls, indicating excellent magnetic softness.

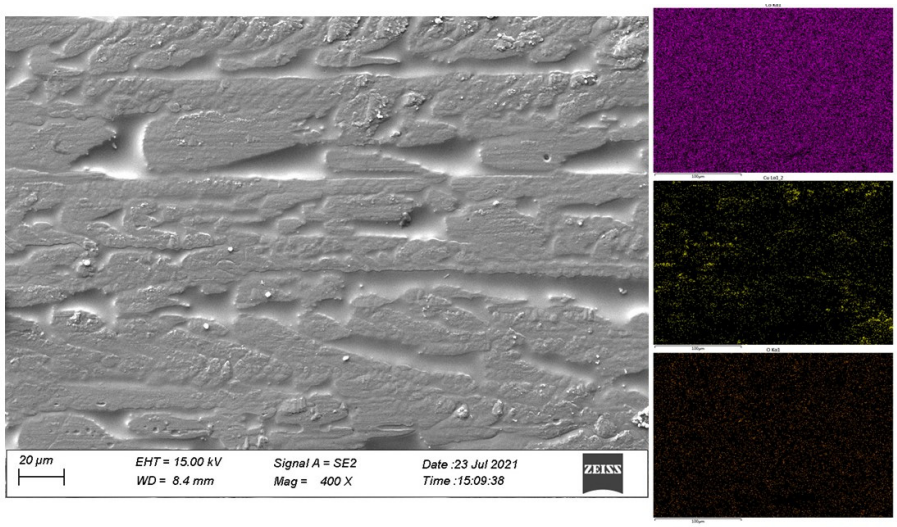
At moderate frequencies, the transverse magnetization mainly proceeds via domain wall displacements, with a single-peak GMI effect, and the GMI response decreases with the H_{ex}. As the frequency increases, the rotation processes become important when H_{ex} is of the order of the effective anisotropy field *Hk*. In the case of a transverse magnetic domain structure, the permeability reaches a peak, requiring much larger longitudinal magnetic fields [7,30]. Consequently, although the GMI ratio is improved after current annealing, the field sensitivity is increased to the highest value at around 1 MHz, and then it decreases, as shown in Figure 4b, due to the impedance peak shifting to a higher magnetic field.

The EDS results for the ribbons, before and after annealing, are shown in Figure 7. A copper and cobalt accumulation in the as-cast and annealed ribbons is observed. The inhomogeneous distribution of copper is related to the ribbon preparation process using a copper roller. Moreover, the areas in which the metal elements gather will be the locations where the oxidation nucleation points are preferentially formed. On the other hand, the local aggregation of nonferromagnetic metallic elements on the ribbon surface may explain the irregularity in the magnetic domains. Before the MOKE investigation, alcohol cleaning and air drying are applied, but no surface polishing treatment is performed on the ribbon surface. Thus, the initial stress, casting defects, and the nonhomogeneous elements distribution remain in their prepared states, and the imperfections will break the continuity of the surface magnetic domains, inducing diverse domain structures, as observed.

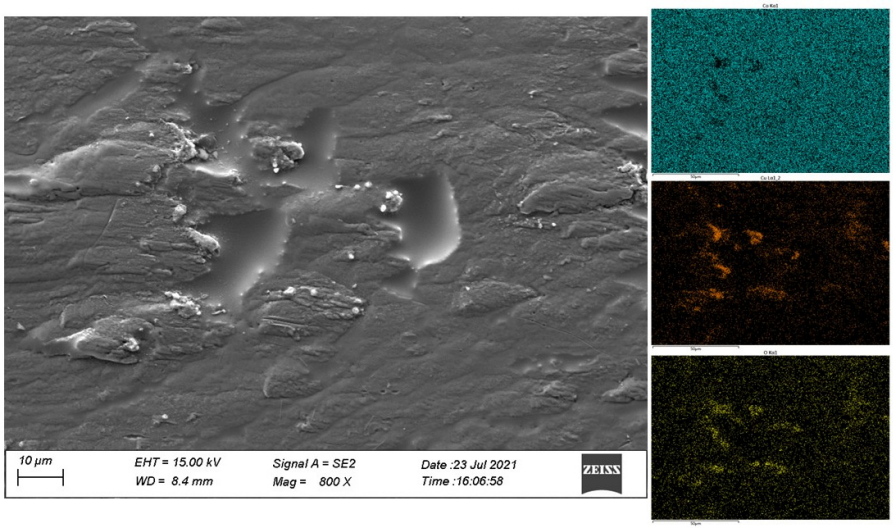


(**a**)

Figure 7. *Cont.*



(**b**)



(**c**)

Figure 7. Surface morphology and elements, Co, Cu, and O, distributed on the ribbon surface: (**a**) as-cast state, (**b**) annealed at 0.3 A, (**c**) annealed at 0.8 A.

However, the presence of the inhomogeneity of the metallic element distribution may lead to the magnetic coupling interaction and change the magnetic anisotropy. This is another notable factor in deducing the complex and irregular domains. Moreover, the surface oxygen content (5.09%) of the annealed ribbon at 0.8 A is significantly higher than that of the as-cast ribbon (2.55%), which is attributable to the surface metallic oxidation process in air with high Joule heat, as observed in the XRD analysis. The oxygen distribution proves again that the formation of metallic hard magnetic phases of oxides is inhomogeneous, and it is related to the metallic element gathering of copper and cobalt. The formation of new phases at sufficiently high temperatures will limit the domain wall movement, owing to the occurrence of many more phase interfaces. Thermodynamically, the crystallization process in amorphous ribbons releases energy and stress, increases crystal anisotropy, and reduces the elastic anisotropy [11]. However, the coupling interaction between the soft magnetic phases of the matrix and the hard magnetic phases of the oxides is generated and enhanced after Joule annealing treatment. The competition between crystal anisotropy and elastic anisotropy causes the rearrangement of the domain structures. Consequently, new regular fingerprint-like domains, with many more domain walls, are formed after annealing at 0.8 A, and the easy magnetization direction gradually becomes longitudinal.

4. Conclusions

The GMI effect of as-cast and Joule annealed Co-ich ribbons at different frequencies is analyzed, considering the surface magnetic domain structures. The as-cast ribbon exhibits an amorphous structure, and its GMI effect is weak. The inhomogeneous distribution of solidification stress and nonferromagnetic element copper induce the irregular magnetic domain structures, with complex anisotropy, in the as-cast ribbon. Joule annealing treatment can optimize the GMI effect of these Co-rich ribbons by the rearrangement of the domains. Stress relaxation and homogenization by Joule heat converts the uneven vortex domains into regular strip-like domains, and the GMI response is improved. Crystallization and the formation of metallic oxides during Joule annealing treatment cause the competition between crystal anisotropy and elastic anisotropy, and the magnetic domains are further refined, owing to the combined effect of thermo stimulation and magnetic field-induced orientation constraint. The transformation of the magnetic domain structures and the increase in transverse magnetic anisotropy improve the GMI effect. Ribbons annealed under 0.8 A exhibit the best GMI effect, with a field sensitivity of 418 and 782%/(kA/m) at 0.2 and 0.8 MHz, respectively. The sensitive field response at frequencies less than 1 MHz allows for the designing of GMI sensors at low working frequencies.

Author Contributions: Writing and preparing the full text is made by S.Z. Part of the figure's arrangement and data analysis are made by Z.G. SEM test and analysis of some experimental data are made by W.C. Some revision of this paper is made by D.Z. All authors have read and agreed to the published version of the manuscript.

Funding: This work is supported by the National Natural Science Foundation of China (No. 51861031).

Data Availability Statement: The data presented in this study are available on request from the corresponding author.

Acknowledgments: The authors would like to express their appreciation to Zhao Zhenjie and Guo Yongbin from East China Normal University for their support and assistance with the GMI experiment. The authors also would like to thank Zhang Kewei and Chen Zhe from Taiyuan University of Science and Technology for their support in the observation of the domain structures.

Conflicts of Interest: The authors declare no conflict of interest.

References

1. Mohri, K.; Kohzawa, T.; Kawashima, K.; Yoshida, H.; Panina, L.V. Magneto-inductive effect (MI effect) in amorphous wires. *IEEE Trans Magn.* **1992**, *28*, 3150–3152. [CrossRef]
2. Melo, L.G.C.; Menard, D.; Yelon, A.; Ding, L.; Saez, S.; Dolabdjian, C. Optimization of the magnetic noise and sensitivity of giant magnetoimpedance sensors. *J. Appl. Phys.* **2008**, *103*, 033903. [CrossRef]
3. Phan, M.H.; Peng, H.X. Giant magnetoimpedance materials:Fundamentals and applications. *Prog. Mater. Sci.* **2008**, *53*, 323–420. [CrossRef]
4. Ding, L.; Saez, S.; Dolabdjian, C.; Luiz, G.C.M.; Yelon, A.; Menard, D. Equivalent Magnetic Noise Limit of Low-Cost GMI Magnetometer. *IEEE Sens. J.* **2009**, *9*, 159–168. [CrossRef]
5. Nematov, M.G.; Baraban, I.; Yudanov, N.A.; Rodionova, V.; Qin, F.X.; Peng, H.X.; Panina, L.V. Evolution of the magnetic anisotropy and magnetostriction in Co-based amorphous alloys microwires due to current annealing and stress-sensory applications. *J. Alloys Compd.* **2020**, *837*, 155584. [CrossRef]
6. Kamruzzaman, M.; Rahman, I.Z.; Rahman, M.A. A review on magneto-impedance effect in amorphous magnetic materials. *J. Mater. Process. Technol.* **2001**, *119*, 312–317. [CrossRef]
7. Guo, H.Q.; Kronmuller, H.; Dragon, T.; Chen, C.; Shen, B.G. Transverse domain structure related giant magnetoimpedance in nanocrystalline $Fe_{73.5}Cu_1Nb_3Si_{13.5}B_9$ ribbons. *J. Appl. Phys.* **1998**, *84*, 5673–5676. [CrossRef]
8. Kraus, L.; Malatek, M.; Postava, K.; Janickovic, P. Asymmetric giant magnetoimpedance in stress-field annealed CoFeBSi amorphous ribbons. *J. Magn. Magn. Mater.* **2005**, *290–291*, 1131–1133. [CrossRef]
9. Turtelli, R.S.; Sinnecker, J.P.; Grossinge, R.; Badurek, G.; Kussbach, C.; Allia, P. Stress dependence of magnetization processes: Reversals and relaxation in $Fe_xCo_{85}ÀxB_{15}$ amorphous ribbons. *Phys. Rev. B* **2001**, *63*, 094427. [CrossRef]
10. Chizhik, A.; Vega, V.; Mohamed Abd El-Moez, A.; Prida, V.M.; Sanchez, T.; Hernando, B.; Ipatov, M.; Zhukova, V.; Zhukov, A.P.; Stupakiewicz, A.; et al. Surface magnetic properties and giant magnetoimpedance effect in Co-based amorphous ribbons. *Intermetallics* **2017**, *86*, 15–19. [CrossRef]

11. Dastani, M.M.; AL-Ali, M.H.; Moradi, M. Influence of current annealing on the magneto-impedance response of cobased ribbons arising from surface structural improvement. *J. Non-Cryst. Solids* **2019**, *516*, 9–13. [CrossRef]
12. Ozturk, S.; Icin, K.; Gencturk, M.; Gobuluk, M.; Topal, U.; Svec, P. Surface and structural characterization of amorphous Fe, Co-based melt-spun ribbons subjected to heat treatment processes. *J. Non-Cryst Solids* **2019**, *522*, 11. [CrossRef]
13. Brunetti, L.; Tiberto, P.; Vinai, F.; Chiriac, H. High-frequency giant magnetoimpedance in joule-heated Co-based amorphous ribbons and wires. *Mater. Sci. Eng. A* **2001**, *304–306*, 961–964. [CrossRef]
14. Menard, D.; Yelon, A. Theory of longitudinal magnetoimpedance in wires. *J. Appl. Phys.* **2000**, *88*, 379–393. [CrossRef]
15. Hernando, A.; Gonzalez, A.P.; Crespo, M.M. Magnetization fluctuations in random anisotropy ferromagnets. *J. Magn. Magn. Mater.* **2004**, *272–276*, 1347–1350. [CrossRef]
16. Gazda, P.; Szewczyk, R. Influence of Joule-Annealing on Double-Peak GMI Effect in Co-Based Amorphous Ribbons. *Acta Phys Pol. A* **2020**, *137*, 818–820. [CrossRef]
17. Zhukov, A.; Ipatov, M.; Corte-Leon, P.; Legarreta, L.G.; Churyukanova, M.; Blanco, J.M.; Gonzalez, J.; Taskaev, S.; Hernando, B.; Zhukova, V. Giant magnetoimpedance in rapidly quenched materials. *J. Alloys Compd.* **2020**, *814*, 152225. [CrossRef]
18. Corte-Leon, P.; Zhukova, V.; Ipatov, M.; Blanco, J.M.; Zhukov, A. Effect of Joule heating on giant magnetoimpedance effect and magnetic properties of Co-rich microwires. *J. Alloys Compd.* **2021**, *883*, 160778. [CrossRef]
19. Corte-Leon, P.; Zhukova, V.; Blanco, J.M.; Ipatov, M.; Taskaev, S.; Churyukanova, M.; Gonzalez, J.; Zhukov, A. Engineering of magnetic properties and magnetoimpedance effect in Fe-rich microwires by reversible and irreversible stress-annealing anisotropy. *J. Alloys Compd.* **2021**, *855*, 157460. [CrossRef]
20. Li, X.P.; Zhao, Z.J.; Chua, C.; Seet, H.L.; Lu, L. Enhancement of giant magnetoimpedance effect of electroplated NiFe/Cu composite wires by dc Joule annealing. *J. Appl. Phys.* **2003**, *94*, 7626–7630. [CrossRef]
21. Coisson, M.; Kane, S.N.; Tiberto, P.; Vinai, F. Influence of DC Joule-heating treatment on magnetoimpedance effect in amorphous Co64Fe21B15 alloy. *J. Magn. Magn. Mater.* **2004**, *271*, 312–317. [CrossRef]
22. Corte-Leon, P.; Zhukova, V.; Ipatov, M.; Blanco, J.M.; Gonzalez, J.; Zhukov, A. Engineering of magnetic properties of Co-rich microwires by joule heating. *Intermetallics* **2019**, *105*, 92–98. [CrossRef]
23. Gonzalez-Alonso, D.; Gonzalez-Legarreta, L.; Corte-Leon, P.; Zhukova, V.; Ipatov, M.; Blanco, J.M.; Zhukov, A. Magnetoimpedance Response and Field Sensitivity in Stress-Annealed Co-Based Microwires for Sensor Applications. *Sensors* **2020**, *20*, 3227. [CrossRef] [PubMed]
24. Celegato, F.; Coisson, M.; Kane, S.N.; Tiberto, P.; Vinai, F. High-frequency magnetoimpedance on annealed amorphous magnetic wires with different magnetostriction constants. *J. Non-Cryst. Solids* **2007**, *353*, 919–921. [CrossRef]
25. Dwevedi, S.; Markandeyulu, G.; Ohodnicki, P.R.; Leary, A.; McHenry, M.E. Stress-MI and domain studies in Co-based nanocrystalline ribbons. *J. Magn. Magn. Mater.* **2011**, *323*, 1929–1933. [CrossRef]
26. Ipatov, M.; Gonzalez-Legarreta, L.; Garcia, J.; Chizhik, A.; Dominguez, L.; Zhukova, V.; Zhukov, A.; Hernando, B.; Gonzalez, J. Induced Giant Magnetoimpedance Effect by Current Annealing in Ultra Thin Co-Based Amorphous Ribbons. *IEEE Trans. Magn.* **2013**, *49*, 1009–1012. [CrossRef]
27. Hoa, N.Q.; Thanh, P.Q.; Yu, S.; Chau, N.; Gam, D.T.H. Large Enhancement of the GMI Effect in Multi-Ferromagnetic Ribbons. *J. Korean Phys. Soc.* **2009**, *54*, 2349–2352. [CrossRef]
28. Corte-Leon, P.; Zhukova, V.; Dominquez, L.; Blanco, J.M.; Ipatov, M.; Chizhik, A.; Zhukov, A.; Gonzalez, J. Giant magnetoimpedance and magneto-optical Kerr effects in $(Co_{63}Ni_{37})_{(75)}Si_{15}B_{10}$ amorphous ribbon. *Intermetallics* **2020**, *125*, 6. [CrossRef]
29. Zhukova, V.; Blanco, J.M.; Ipatov, M.; Gonzalez, J.; Churyukanova, M.; Zhukov, A. Engineering of magnetic softness and giant magnetoimpedance effect in Fe-rich microwires by stress-annealing. *Scr. Mater.* **2018**, *142*, 10–14. [CrossRef]
30. Qikui, M.; Yunzhang, F.; Huaijun, S.; Fangmin, Y. A new type of longitudinally driven GMI effect of FeCo-based alloy. *Chin. Sci. Bull.* **2008**, *53*, 329–334.

Disclaimer/Publisher's Note: The statements, opinions and data contained in all publications are solely those of the individual author(s) and contributor(s) and not of MDPI and/or the editor(s). MDPI and/or the editor(s) disclaim responsibility for any injury to people or property resulting from any ideas, methods, instructions or products referred to in the content.